

On the properties of synchrotron-like X-ray emission from laser wakefield accelerated electron beams

C. McGuffey, W. Schumaker, T. Matsuoka, V. Chvykov, F. Dollar, G. Kalintchenko, S. Kneip, Z. Najmudin, S. P. D. Mangles, M. Vargas, V. Yanovsky, A. Maksimchuk, A. G. R. Thomas, and K. Krushelnick

Citation: *Physics of Plasmas* **25**, 043104 (2018); doi: 10.1063/1.5024547

View online: <https://doi.org/10.1063/1.5024547>

View Table of Contents: <http://aip.scitation.org/toc/php/25/4>

Published by the [American Institute of Physics](#)

Articles you may be interested in

[Plasma block acceleration based upon the interaction between double targets and an ultra-intense linearly polarized laser pulse](#)

Physics of Plasmas **25**, 043102 (2018); 10.1063/1.5024032

[Effect of injection-gas concentration on the electron beam quality from a laser-plasma accelerator](#)

Physics of Plasmas **25**, 043106 (2018); 10.1063/1.5008561

[A review of low density porous materials used in laser plasma experiments](#)

Physics of Plasmas **25**, 030501 (2018); 10.1063/1.5009689

[Combined action of corrugation and Weibel instabilities from electron-beam interaction with laser-irradiated plasma](#)

Physics of Plasmas **25**, 033112 (2018); 10.1063/1.5020869

[Astrophysical particle acceleration mechanisms in colliding magnetized laser-produced plasmas](#)

Physics of Plasmas **24**, 092901 (2017); 10.1063/1.4993204

[Intense single attosecond pulse generation from near-critical-density plasmas irradiated by a few-cycle laser pulse](#)

Physics of Plasmas **25**, 023302 (2018); 10.1063/1.5013057



**COMPLETELY
REDESIGNED!**

**PHYSICS
TODAY**

Physics Today Buyer's Guide
Search with a purpose.

On the properties of synchrotron-like X-ray emission from laser wakefield accelerated electron beams

C. McGuffey,^{1,a)} W. Schumaker,¹ T. Matsuoka,^{1,b)} V. Chvykov,¹ F. Dollar,^{1,c)}
 G. Kalintchenko,¹ S. Kneip,² Z. Najmudin,² S. P. D. Mangles,² M. Vargas,¹ V. Yanovsky,¹
 A. Maksimchuk,¹ A. G. R. Thomas,¹ and K. Krushelnick¹

¹Center for Ultrafast Optical Science, University of Michigan, Ann Arbor, Michigan 48109-2099, USA

²The Blackett Laboratory, Imperial College London, London SW7 2BZ, United Kingdom

(Received 1 February 2018; accepted 14 March 2018; published online 3 April 2018)

The electric and magnetic fields responsible for electron acceleration in a Laser Wakefield Accelerator (LWFA) also cause electrons to radiate x-ray photons. Such x-ray pulses have several desirable properties including short duration and being well collimated with tunable high energy. We measure the scaling of this x-ray source experimentally up to laser powers greater than 100 TW. An increase in laser power allows electron trapping at a lower density as well as with an increased trapped charge. These effects resulted in an x-ray fluence that was measured to increase non-linearly with laser power. The fluence of x-rays was also compared with that produced from $K\alpha$ emission resulting from a solid target interaction for the same energy laser pulse. The flux was shown to be comparable, but the LWFA x-rays had a significantly smaller source size. This indicates that such a source may be useful as a backlighter for probing high energy density plasmas with ultrafast temporal resolution. *Published by AIP Publishing.* <https://doi.org/10.1063/1.5024547>

I. INTRODUCTION

Using magnetic insertion devices to generate high frequency synchrotron radiation in the soft x-ray regime requires acceleration of electrons to GeV energies, which can be achieved with existing technology through the use of linear accelerators that are tens of meters long. Beyond the accelerator, the insertion device, which undulates the beam causing it to radiate, may also be many meters long. In contrast, Laser Wakefield Acceleration (LWFA) can achieve similar acceleration and concomitant radiation over mere millimeters. LWFA can produce monoenergetic beams¹ when electrons are accelerated by the strong electric fields associated with relativistic plasma waves driven by a high power short pulse laser. Electron beams generated in this manner can have GeV energy,² and so may also be useful for generating short wavelength radiation through various means such as injection into an undulator³ or by back-scattering laser light.^{4,5} However, the advantage of the LWFA scheme in compactness can be compounded further because the electric fields in the plasma wake can also cause the beam to undulate simultaneously, making an external insertion device unnecessary. The relevant spatial scale in this case is the wavelength of the betatron oscillations, $\lambda_\beta = \lambda_p(2\gamma)^{1/2}$ rather than the spacing of magnets in an undulator, $\mathcal{O}(\text{cm})$. In this equation, γ is the relativistic Lorentz factor of the wakefield accelerated electron beam and λ_p is the relativistic plasma wavelength. Due to the inherently microscopic scale of this undulator, electrons in a LWFA radiation source produce higher frequency radiation as compared to electron beams of

a similar energy in a conventional magnetic insertion device. This radiation (sometimes referred to in the literature as betatron radiation, as it results from the betatron oscillations of the electron in the wakefield cavity) can be highly directional and extremely bright.

Betatron motion has been studied theoretically in an ion channel^{6,7} or bubble,⁸ and in simulation⁹ and has been measured experimentally,^{10–14} with recent measurements of the photon distribution^{15,16} and demonstration of its use as a diagnostic of beam emittance.¹⁷ The wiggler parameter for betatron oscillations is $K_\beta = \sqrt{2}\gamma\pi r_0/\lambda_p$, where r_0 is the spatial amplitude of the betatron motion. In LWFA experiments, the radiated wavelength and strength parameter vary with time and typically, the wiggler parameter is large, $K_\beta > 1$, although some experiments have inferred smaller wiggler parameters.¹⁸ The spectrum in the case of large K_β is expected to be synchrotron-like, with a broad spectrum peaking near the critical photon energy

$$E_c = 6\pi^2\hbar c \frac{\gamma^3 r_0}{\lambda_\beta^2}.$$

Recently some of the potential advantages of using laser-driven betatron sources have been demonstrated. For example, in Ref. 19 the radiation source size was inferred to be $\sim 1 \mu\text{m}$. Betatron radiation generated from LWFA conducted in the bubble regime was also recently investigated in Ref. 20, in which the radiation from a 10 mm gas jet target was measured using a CCD camera. The measured radiation was found to have significantly higher peak brightness (10^{22} photons/s/mm²/mrad²/0.1%BW) than previous measurements and the peak brightness of the betatron radiation was shown to be as high as 3rd generation synchrotron facilities. The radiation spectrum in

^{a)}Present address: University of California, San Diego, San Diego, CA 92093, USA.

^{b)}Present address: Osaka University, Osaka, Japan.

^{c)}Present address: University of California, Irvine, CA 92697, USA.

that case was measured with low resolution using x-ray filters.

In this paper, we discuss systematic measurements of the x-ray fluence and the x-ray spectrum using single-hit photon-counting measurements.²¹ The data cover a wide range of laser power (30–120) TW, and densities ($0.5\text{--}2.1 \times 10^{19} \text{ cm}^{-3}$). Measurements were taken using a deep depletion CCD camera (Andor DO934P-BR-DD), which is less sensitive to photons with energy $\hbar\omega < 2 \text{ keV}$ and more sensitive over the range 3–20 keV as compared to the previous measurements.²⁰ All data were taken with a 360 nm Al filter positioned over the camera as well as Mylar filters of differing thickness. The detector, having 1024×1024 pixels of size $13 \times 13 \mu\text{m}^2$, was placed at 2.8 m distance from the front of the target gas nozzle, and therefore subtended a solid angle of $4.77 \times 4.77 \pm 0.01 \text{ mrad}^2$. This solid angle is smaller than the full-width-at-half-maximum (FWHM) beam divergence (found previously in Ref. 20 to be $4 \times 13 \text{ mrad}^2$) and was comparable to the shot-to-shot pointing stability of the x-ray beam.

The measured signal varied from shot-to-shot during these experiments and it was necessary to average over several shots to observe scaling trends. This is perhaps because as mentioned above the detector acceptance angle was comparable to the pointing stability. Because of the linearity of the detector (1% maximum deviation), the signal above readout noise integrated over the detector is a good indicator of the total energy in x-rays within the response window of the detector and the filter system (roughly 3–20 keV) although the number of photons can only be calculated from these data by making assumptions about the photon energy spectrum. If the x-ray spectra change significantly from shot-to-shot, particularly if the spectra have a critical energy around 4–5 keV (below which the transmission of Mylar drops), this would also contribute to the observed variation. Additionally, the x-ray beam divergence is likely to be sensitive to the electron beam divergence, energy, and source size which all vary somewhat from shot-to-shot and depend on experimental parameters such as density.

All experiments were taken using the HERCULES laser at the Center for Ultrafast Optical Science at the University of Michigan, a Ti:Sapphire laser system with central wavelength 810 nm and minimum pulse duration 35 fs. The laser was focused using an $f/10$ off-axis parabolic mirror to a

focal spot of $12 \mu\text{m}$ FWHM. Using these parameters, electron beams produced by Laser Wakefield Acceleration in the bubble regime at the lower densities were investigated, as well as forced wakefield acceleration in the higher density regime.²² The setup is shown in Fig. 1. The electron beam charge and spectrum were measured using a 0.8 T magnet and a Lanex scintillating screen. Typical electron spectra are shown in Fig. 2. The source size was measured from the x-ray shadow, first of standard radiography targets as shown in Fig. 1 (inset) and then, using the cleaved edge of an InSb crystal. The radiation was also previously found to exhibit spatial coherence, enabling high resolution phase contrast imaging of dense objects.²³

II. X-RAY SCALING MEASUREMENTS

In Fig. 3(a), the total x-ray fluence (energy per unit solid angle) (blue) and the electron charge (green) are plotted for 17 single shots. These data were taken with a 5 mm nozzle and laser power $58.4 \pm 2.5 \text{ TW}$. The notable correlation between fluence and beam charge indicates that nearly all of the accelerated relativistic electrons contribute to the x-ray radiation. The correlation is further shown in Fig. 3(c). The overall shape of the charge curve as a function of density has been observed repeatedly in previous LWFA experiments with the HERCULES laser—an initial rise in charge above the injection threshold density followed by a steep fall off in charge as plasma density is increased beyond the condition $\lambda_p < c\tau$. The two highest fluence data points from the 5 mm data, which stand out above the rest, are distinguished from the other shots because the electron spectra were much more monoenergetic, with most of the charge in the highest energy part of the beam. As shown in (b) and (d), the x-ray fluence depends not only on beam charge, but also on the average energy of the beam. Figure 4(a) shows the x-ray total energy fluence, F , as a function of density for three laser power settings. Each data point gives the fluence averaged over several shots (up to 16) under identical experimental conditions and the error bars span one standard deviation of those shots. Shots with $Q < 20 \text{ pC}$ electron beam charge were excluded.

The rise and fall in x-ray fluence with increasing density within each power data set curve are due in part to the trend in trapped electron beam charge as a function of density discussed above [see Fig. 3(a)]. As laser power is increased, x-rays can be generated at lower density and the total x-ray

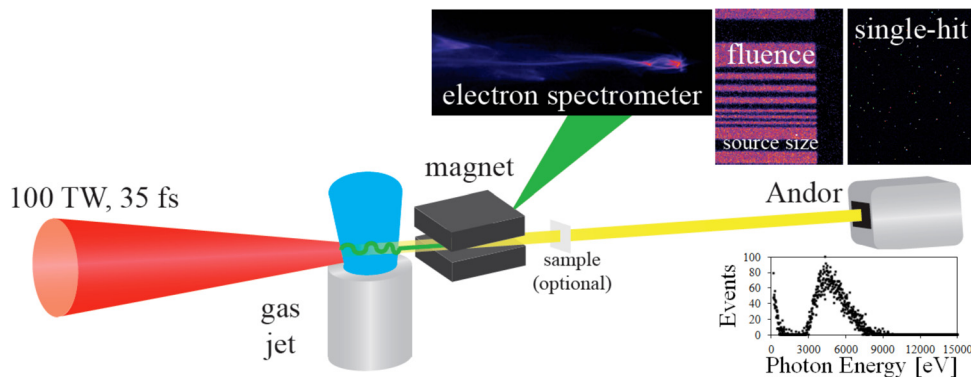


FIG. 1. Experimental setup.

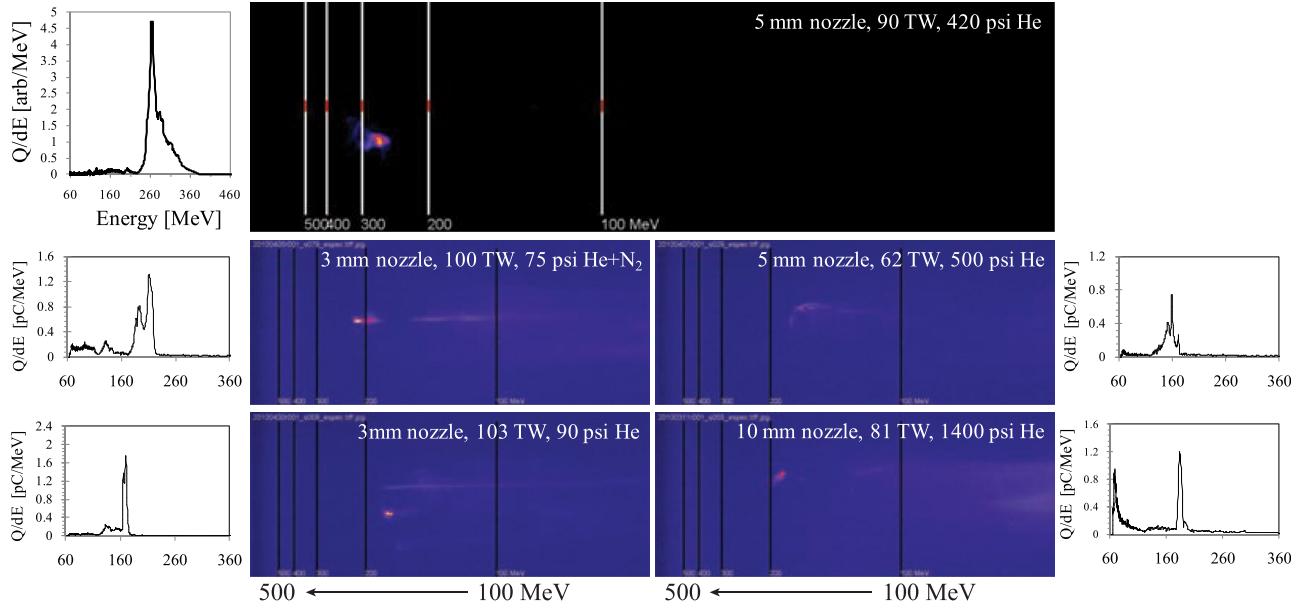


FIG. 2. Example spectra of monoenergetic electron shots produced for 5 mm and 10 mm gas nozzle lengths in this experiment.

energy increases more than linearly (see the inset, which plots the highest fluence from the three data sets). These effects can be explained by considering the effect of laser power on the LWFA process. As found in a series of experiments with the HERCULES laser and covering the same parameter space,²⁴ the threshold injection density scales as $n_{inj} \propto P^{-0.8}$, and the maximum energy gain scales inversely with density $E_{max} \propto n^{-1.4}$. These findings are in qualitative agreement with theoretical predictions.^{8,25} The beam charge has also been observed to increase with power. Considering that $\lambda_\beta \propto \gamma^{-3/2}$ and $E_c \propto \gamma^2 r_0$, it is consequently expected that the x-ray energy fluence should increase non-linearly with power. From the analytical model constructed in Ref. 8, the radiated energy from electrons accelerated in a bubble-shaped potential is

$$E_{rad} = \frac{L_{int}}{3^{3/4}} \frac{\omega_0}{c} \left(\frac{n_c}{n_e} \right)^{1/4} a_0^{9/2} m_e c^2. \quad (1)$$

The radiation cone is assumed to narrow with increasing gamma, giving a fluence density $F_{rad} \propto E_{rad}/\theta^2 \propto E_{rad}\gamma^2$. Here, we assume that the laser is self-focused, consistent with operation in the bubble regime, $a_0 = 2(P/P_{crit})^{1/3} (n_e/n_c)^{1/3}$ and also that the electron energy is governed by the density, $\gamma = 2a_0(n_c/n_e)$. Combining these expressions yields

$$F_{rad} \propto L_{int} \left(\frac{P}{P_{crit}} \right)^{13/6} \left(\frac{n_c}{n_e} \right)^{1/12} \propto P^{2.2}, \quad (2)$$

which is close to the empirical scaling in derived from the data in the inset to Fig. 4.

Additionally, the x-ray spectra were measured using the Andor CCD where the x-ray fluence was controlled such that each pixel of the CCD on average measured less than 1 photon. This was achieved primarily by using Mylar and/or metal filters and by increasing the detector distance from the

source. The extended separation also helps to evenly illuminate the detector but makes pointing fluctuations more problematic. In this “single-hit” regime, the signal from a single pixel could be attributed to a single photon, with signal proportional to the photon energy. For this measurement, many pixels are needed. The detector energy scale was calibrated using both Fe-55 and Am-241 radioactive sources. The histograms taken from the single-hit data indicate single shot fluence as high as 10^{11} photons per steradian within the range 4–20 keV averaged over the detector ($2-3 \times 10^{-5}$ sr), though the beam appears to be much larger than the detector area on many shots.

Several spectra are compared in Fig. 4. The data presented here were taken with a 3 mm nozzle and 100.0 ± 4.7 TW laser power. The gas jet backing pressure was varied. The electron beams had maximum energies ranging from 165 to 226 MeV with either broad or monoenergetic electron spectra. As shown in the logarithmic plot, the radiated spectra can broadly be described by assigning a single photon effective temperature. From the data in this figure, no trend in the effective temperature is obvious and from the entire dataset, the effective temperature appears to be insensitive to experimental parameters. Adjusted for the temperature, the qualitative shape of the x-ray spectrum did not change significantly and could be well described by a synchrotron-like spectrum rather than an undulator spectrum consisting of broadened harmonics.

The spectral data reaffirm the flux dependence on charge and energy observed in the fluence measurements. The dominant trend in Fig. 4 is that x-ray fluence increases with charge. However, the exceptions are those shots that have broad electron energy spectra. The electrons with low energy in the broad spectrum shots produced fewer photons within the detection spectral window. When normalized to charge (not shown), the signal from the 197 pC shot, which had a broad spectrum and the lowest maximum energy of all the shots, falls below all the other curves.

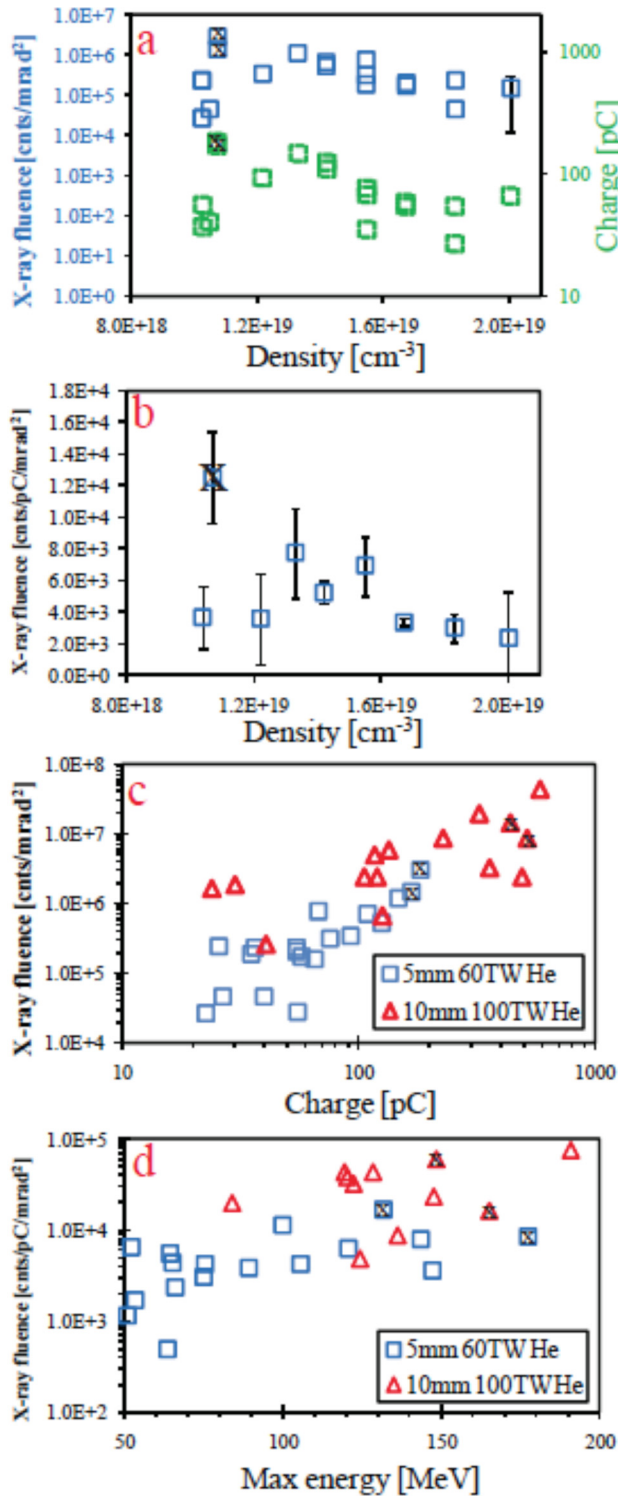


FIG. 3. Correlation is observed (a) between x-ray fluence (blue) and electron beam charge (green) for 17 shots using a 5 mm nozzle and 60 TW. Dependence on charge is further shown in (c). In (b), the data have been normalized by charge (and averaged in each bin). Two shots in which the beam was monoenergetic at high energy (marked by “x”) stand out when normalized to charge, i.e., these beams had higher charge-averaged energy than the other beams. As shown in (d), the fluence also increases with maximum beam energy.

III. COMPARISON OF THE LWFA X-RAY SOURCE WITH $K\text{-}\alpha$ EMISSION FROM A COPPER TARGET

Despite typically having a broad spectrum, the LWFA x-ray source has several important advantages as compared

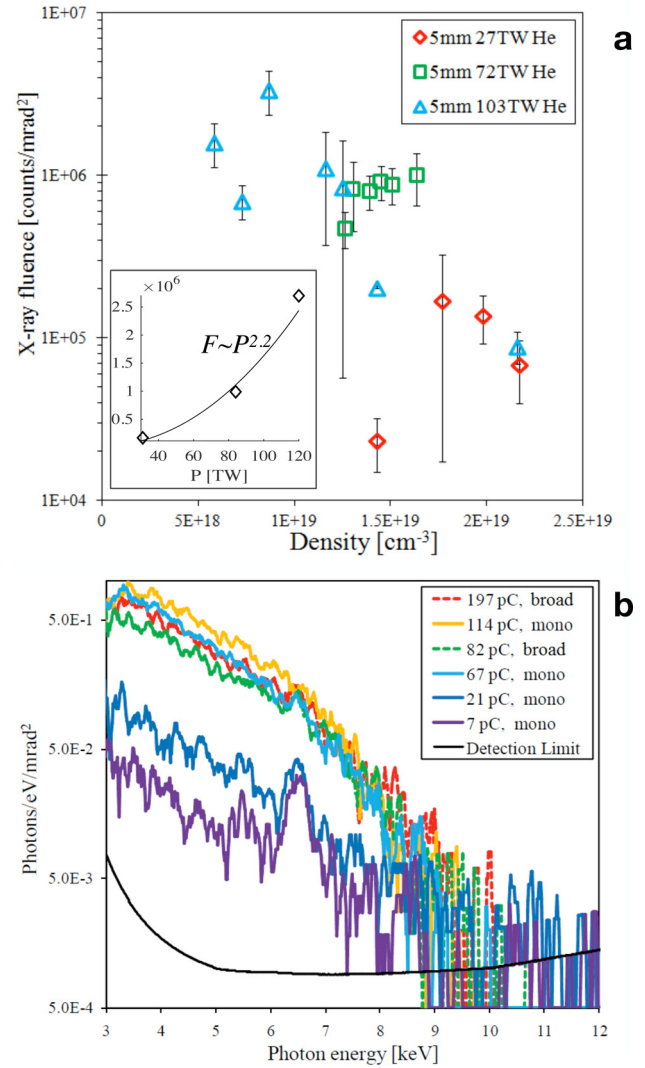


FIG. 4. (a) Scans of x-ray fluence (note logarithmic scale) as a function of density for three laser power settings. Each point is the average of a trial at fixed density. The rise and fall of each curve with increasing density are characteristic of the trend in trapped electron beam charge. The inset plot (linear) shows the maximum trial fluence at each power level shown in the main graph, with a black line showing the curve power fitting with a trend line $F \propto P^{2.2}$. (b) X-ray spectra acquired using the Andor CCD camera in single-hit operation. The feature at 6.4 keV is the $K\text{-}\alpha$ line of iron likely produced from energetic electrons colliding with the vacuum chamber walls.

to other x-ray sources with regard to directionality, source size, and pulse duration for many applications. One of the most common laser driven sources for x-ray backlighting and x-ray probing of plasma is the $K\text{-}\alpha$ source. For $K\text{-}\alpha$ photon production, an intense laser is focused onto a material and the energetic electrons produced during the interaction collide with the ions, causing an inner shell electron to be ionized from atoms in the target material. $K\text{-}\alpha$ photon emission, corresponding to emission of a photon during the de-excitation of an L-shell electron to the vacant K-shell, is the most likely result, especially for low-Z materials. In a material like copper, the electrons can continue to generate K-shell vacancies for picoseconds after the interaction.²⁶ In our experiments, we were able to directly compare the LWFA x-ray source with the characteristics of a copper $K\text{-}\alpha$ source for the same power laser, by using an identical experimental

setup simply by placing a copper target of 50 or 100 μm thickness in the position of the gas jet focus. In this way, we could compare the total flux of x-ray photons and the spectrum as well as the image resolution of either a $K\text{-}\alpha$ x-ray source or LWFA x-ray source which could be used as a backlighter with the same energy laser.

Figure 5 shows the signal on an x-ray sensitive CCD camera for 4 shots under varying conditions. In these experiments, several different filters were used in front of the x-ray camera. In addition, a 10 μm thick copper mesh was placed between the x-ray source and the detector. The transmission properties of the various filters are also shown in Fig. 5. In Fig. 5(a), an image taken with the LWFA x-ray source is shown using “self-injection,” i.e., the target gas was pure helium. In Fig. 5(b), the target gas was a mixture of helium and a 5% component of nitrogen. The use of a small amount of nitrogen dopant enables an increase in the charge of the electron beam generated due to the additional process of ionization injection of electrons into the laser produced wakefield,²⁷ which then contributes to the charge of the accelerated electron beam. Finally, Fig. 5(c) shows the image taken with the $K\text{-}\alpha$ source as a comparison. In all the images, various metal filters overlay the image, with the transmission curves shown in Figs. 5(d) and 5(e).

It is clear from Fig. 5 that the source size is greatly increased in Fig. 5(c) compared with Fig. 5(a) and Fig. 5(b). Clearly, the x-ray source size using the $K\text{-}\alpha$ emission is much larger than the 10 μm size of the mesh such that it cannot be resolved using the backlighting technique. This confirms that the source size of the $K\text{-}\alpha$ is significantly larger than that of the LWFA x-ray emission. This is due to the hot electrons spreading out from the small focal spot interaction and either refluxing or propagating along the surface in the

strong electromagnetic fields generated at the surfaces.²⁵ In Fig. 5(f), the source size measured using an InSb cleaved crystal (by fitting an error function) is plotted as a function of density for both pure helium and helium with a 5% component of nitrogen. There is no clear difference in the source size for “ionization-injection” and “self-injection,” and the trend with density is weaker than the shot-to-shot variation in the source size.

In these experiments, we also used a curved quartz crystal to image the x-rays produced from both the LWFA x-ray source and the $K\text{-}\alpha$ source. The reflectivity of the crystal was chosen to be optimized for collection of the copper $K\text{-}\alpha$ line at 8.048 keV. The experimental set-up is shown in Fig. 6(a). Image plates sensitive to 8 keV photons were used as the detector in these shots. The data are shown in Figs. 6(b) and 6(c). It is clear from these data that despite the LWFA x-ray radiation having a much broader spectrum, it has a sufficient flux of x-rays/steradian within the reflectivity range of the curved crystal to enable efficient diffraction and focusing even when compared to a $K\text{-}\alpha$ source. Note also that the $K\text{-}\alpha$ source emits photons isotropically and typically has a pulse duration of a picosecond or longer compared to emission from the LWFA, which can have an x-ray pulse duration even less than the laser duration.

IV. DISCUSSION AND CONCLUSIONS

In conclusion, the increase in accelerated charge and maximum energy gain made possible by an increase in laser power means that the total x-ray energy radiated from betatron oscillations in LWFA scales much faster than linearly with laser power. The radiated energy varies nearly linearly with charge as would be expected for independently radiating electrons. In the ideal case of a laser wake-field

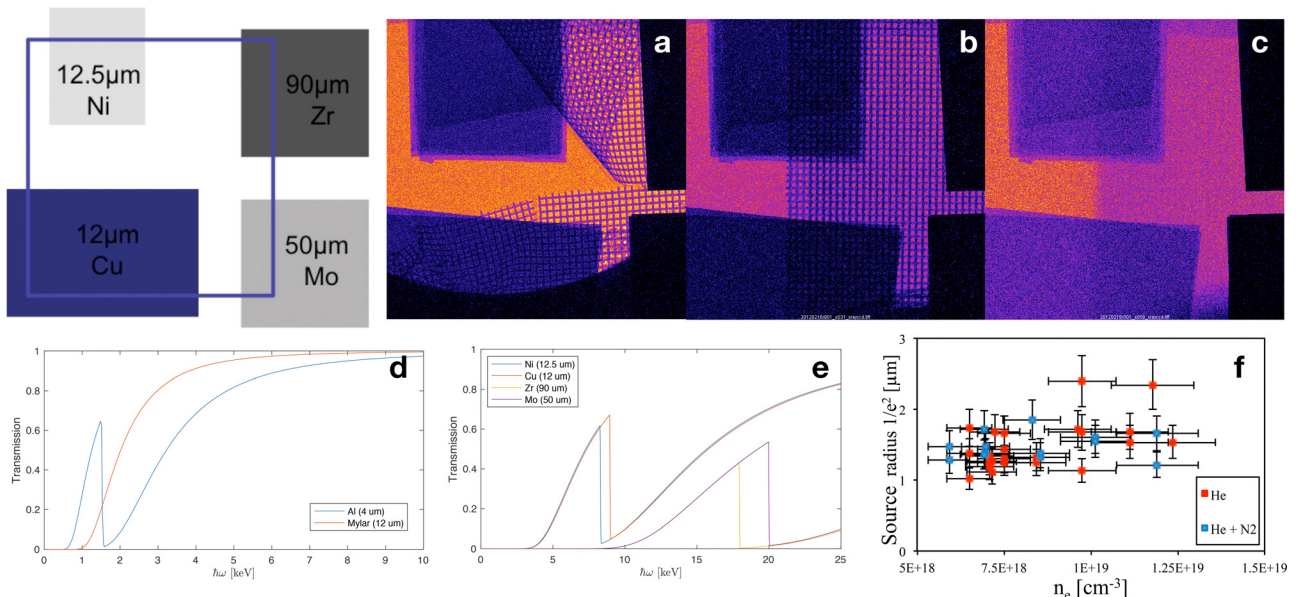


FIG. 5. Direct comparison of the x-ray flux from several laser generated sources. The top panels show the x-ray transmission through various metal filters and a copper mesh, with the configuration of filters shown to the left. (a) Helium gas target (“self-injection”) and (b) helium and nitrogen mixed gas target (“ionization injection”). (c) $K\text{-}\alpha$ source from a 10 μm thick copper target. Note that the 50 μm copper mesh superimposed over the filters is resolved in (a) and (b) but is not resolved in (c). (d) and (e) The photon energy dependent transmissions of the various filters. (f) The source radius as a function of density for helium gas target (red) and the helium and nitrogen mixed gas target (blue) measured using a cleaved InSb crystal.

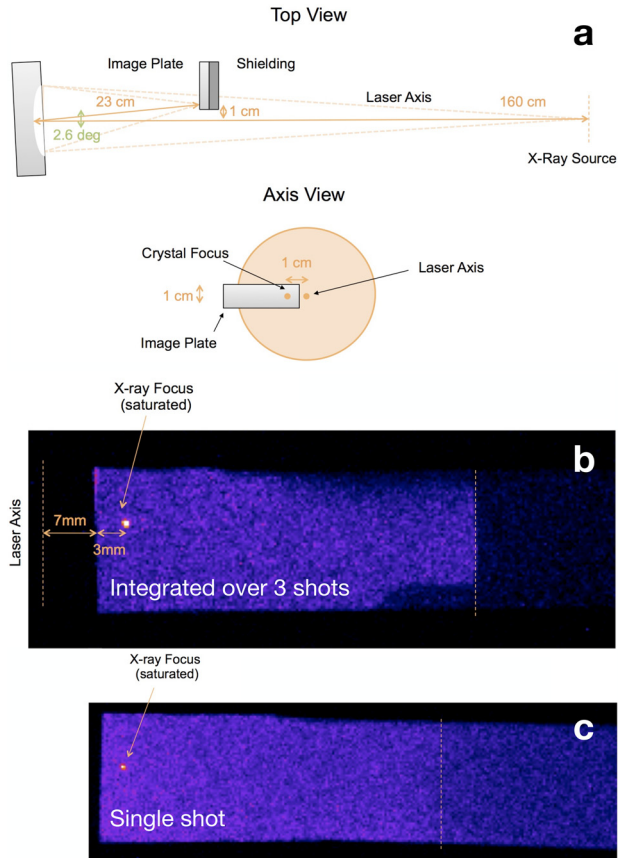


FIG. 6. (a) The experimental setup for collection and imaging of x-rays using a curved crystal imager, designed for use with the 8 keV copper $K\alpha$ line. (b) and (c) Two raw images from an image plate detector showing the focused x-rays produced using the setup in (a). (b) Using a copper $K\alpha$ target, with signal integrated over 3 shots and (c) is using the LWFA x-ray source.

accelerator that generates a monoenergetic beam at the highest possible energy, the radiated energy fluence is maximized per unit charge. However, the total fluence may be increased further in the event of beam driven acceleration that can trap additional charge, and also beam driven instabilities, which can cause the emission of additional radiation. The radiated spectrum was measured directly, showing a smooth synchrotron-like spectrum with photon energies in the keV range from a few mm laser wakefield accelerator generating electron beams with 100s of pC charge and maximum energy 192 MeV. No evidence of radiation in a low wiggler parameter (undulator) regime was measured under these experimental conditions. We have also shown that the x-ray fluence is similar to that produced from $K\alpha$ emission generated by interaction with a Cu target using a spherically curved crystal collection optic in a similar experimental setup. The LWFA x-ray source has a much broader spectrum, enabling its use as a wavelength-selectable backlighter and it has additional advantages due to its much smaller source size and high directionality. This source is expected to have pulse durations even shorter than the laser pulse duration which can enable pump-probe measurements with femtosecond temporal resolution. These measurements therefore demonstrate that the LWFA x-ray source may be useful as a backlighter for time and space resolved probing of high energy density plasmas.

ACKNOWLEDGMENTS

This work was supported by the DHS/DNDO (Award No. F021166), the NSF through Award Nos. 1054164 and 0935197, DARPA under Contract Nos. N66001-11-1-4208, and the DOE/NNSA DE-NA0002372.

- ¹S. P. D. Mangles, C. D. Murphy, Z. Najmudin, A. G. R. Thomas, J. L. Collier, A. E. Dangor, P. S. Foster, J. L. Collier, E. J. Divall, J. G. Gallacher, C. J. Hooker, D. A. Jaroszynski, A. J. Langley, W. B. Mori, P. A. Norreys, F. S. Tsung, R. Viskup, B. R. Walton, and K. Krushelnick, *Nature* **431**, 535 (2004); C. G. R. Geddes, C. Toth, J. van Tilborg, E. Esarey, C. B. Schroeder, D. Bruhwiler, C. Nieter, J. Cary, and W. P. Leemans, *ibid.* **431**, 538 (2004); J. Faure, Y. Gilneec, A. Pukhov, S. Kiselev, S. Gordienko, E. Lefebvre, J.-P. Rousseau, F. Burgy, and V. Malka, *ibid.* **431**, 541 (2004).
- ²C. E. Clayton, J. E. Ralph, F. Albert, R. A. Fonseca, S. H. Glenzer, C. Joshi, W. Lu, K. A. Marsh, S. F. Martins, W. B. Mori, A. Pak, F. S. Tsung, B. B. Pollock, J. S. Ross, L. O. Silva, and D. H. Froula, *Phys. Rev. Lett.* **105**, 105003 (2010).
- ³M. Fuchs, R. Weingartner, A. Popp, Z. Major, S. Becker, J. Osterhoff, I. Cortrie, B. Z. R. Horlein, G. D. Tsakiris, U. Schramm, T. P. Rowlands-Rees, S. M. Hooker, D. Habs, F. Krausz, and F. Gruner, *Nat. Phys.* **5**, 826 (2009).
- ⁴R. W. Schoenlein, W. P. Leemans, A. H. Chin, P. Volfbeyn, T. E. Glover, P. Balling, M. Zolotarev, K.-J. Kim, S. Chattopadhyay, and C. V. Shank, *Science* **274**, 236 (1996).
- ⁵G. Sarri, D. J. Corvan, W. Schumaker, J. M. Cole, A. Di Piazza, H. Ahmed, C. Harvey, C. H. Keitel, K. Krushelnick, S. P. D. Mangles, Z. Najmudin, D. Szymes, A. G. R. Thomas, M. Yeung, Z. Zhao, and M. Zepf, *Phys. Rev. Lett.* **113**, 224801 (2014).
- ⁶E. Esarey, B. A. Shadwick, P. Catravas, and W. P. Leemans, *Phys. Rev. E* **65**, 056505 (2002).
- ⁷K. Ta Phuoc, S. Corde, R. Fitour, R. Shah, F. Albert, J. P. Rousseau, F. Burgy, A. Rousse, V. Seredov, and A. Pukhov, *Phys. Plasmas* **15**, 073106 (2008).
- ⁸A. G. R. Thomas, *Phys. Plasmas* **17**, 056708 (2010).
- ⁹A. G. R. Thomas and K. Krushelnick, *Phys. Plasmas* **16**, 103103 (2009).
- ¹⁰K. Ta Phuoc, S. Corde, R. Shah, F. Albert, R. Fitour, J.-P. Rousseau, F. Burgy, B. Mercier, and A. Rousse, *Phys. Rev. Lett.* **97**, 225002 (2006).
- ¹¹Y. Glinec, J. Faure, A. Lifschitz, J. M. Vieira, R. A. Fonseca, L. O. Silva, and V. Malka, *Europhys. Lett.* **81**, 64001 (2008).
- ¹²A. Rousse, K. Ta Phuoc, R. Shah, A. Pukhov, E. Lefebvre, V. Malka, S. Kiselev, F. Burgy, J.-P. Rousseau, D. Umstadter, and D. Hulin, *Phys. Rev. Lett.* **93**, 135005 (2004).
- ¹³S. Kneip, S. R. Nagel, C. Bellei, N. Bourgeois, A. E. Dangor, A. Gopal, R. Heathcote, S. P. D. Mangles, J. R. Marques, A. Maksimchuk, P. M. Nilson, K. Ta Phuoc, S. Reed, M. Tzoufras, F. S. Tsung, L. Willingale, W. B. Mori, A. Rousse, K. Krushelnick, and Z. Najmudin, *Phys. Rev. Lett.* **100**, 105006 (2008).
- ¹⁴S. Cipiccia, M. R. Islam, B. Ersfeld, R. P. Shanks, E. Brunetti, G. Vieux, X. Yang, R. C. Issac, S. M. Wiggins, G. H. Welsh, M.-P. Anania, D. Maneuski, R. Montgomery, G. Smith, M. Hoek, D. J. Hamilton, N. R. C. Lemos, D. Szymes, P. P. Rajeev, V. O. Shea, J. M. Dias, and D. A. Jaroszynski, *Nat. Phys.* **7**, 867 (2011).
- ¹⁵S. Corde, C. Thauray, K. T. Phuoc, A. Lifschitz, G. Lambert, J. Faure, O. Lundh, E. Benveniste, A. Ben-Ismaïl, L. Arantchuk, A. Marciniak, A. Stordeur, P. Brijesh, A. Rousse, A. Specka, and V. Malka, *Phys. Rev. Lett.* **107**, 215004 (2011).
- ¹⁶F. Albert, B. B. Pollock, J. L. Shaw, K. A. Marsh, J. E. Ralph, Y.-H. Chen, D. Alessi, A. Pak, C. E. Clayton, S. Glenzer, and C. Joshi, *Phys. Rev. Lett.* **111**, 235004 (2013).
- ¹⁷S. Kneip, C. McGuffey, J. L. Martins, M. S. Bloom, V. Chvykov, F. Dollar, R. Fonseca, S. Jolly, G. Kalintchenko, K. Krushelnick, A. Maksimchuk, S. P. D. Mangles, Z. Najmudin, C. A. J. Palmer, K. T. Phuoc, W. Schumaker, L. O. Silva, J. Vieira, V. Yanovsky, and A. G. R. Thomas, *Phys. Rev. ST Accel. Beams* **15**, 021302 (2012); M. Schnell, A. Svert, B. Landgraf, M. Reuter, M. Nicolai, O. Jckel, C. Peth, T. Thiele, O. Jansen, A. Pukhov, O. Willi, M. C. Kaluza, and C. Spielmann, *Phys. Rev. Lett.* **108**, 075001 (2012).
- ¹⁸G. R. Plateau, C. G. R. Geddes, D. B. Thorn, M. Chen, C. Benedetti, E. Esarey, A. J. Gonsalves, N. H. Matlis, K. Nakamura, C. B. Schroeder, S. Shiraishi, T. Sokollik, J. van Tilborg, C. Toth, S. Trotsenko, T. S. Kim, M.

- Battaglia, T. Sthlker, and W. P. Leemans, *Phys. Rev. Lett.* **109**, 064802 (2012).
- ¹⁹F. Albert, R. Shah, K. Ta Phuoc, R. Fitour, F. Burgy, J.-R. Rousseau, A. Tafzi, D. Douillet, T. Lefrou, and A. Rousse, *Phys. Rev. E* **77**, 056402 (2008).
- ²⁰S. Kneip, C. McGuffey, J. L. Martins, S. F. Martins, C. Bellei, V. Chvykov, F. Doillar, R. Fonseca, C. Huntington, G. Kalintchenko, A. Maksimchuk, S. P. D. Mangles, T. Matsuoka, S. R. Nagel, C. Palmer, J. Schreiber, K. Ta Phoac, A. G. R. Thomas, V. Yanovsky, L. O. Silva, K. Krushelnick, and Z. Najmudin, *Nat. Phys.* **6**, 980–983 (2010).
- ²¹S. Fourmaux, S. Corde, K. Ta Phuoc, P. M. Leguay, S. Payeur, P. Lassonde, S. Gnedyuk, G. Lebrun, C. Fourment, V. Malka, S. Sebban, A. Rousse, and J. C. Kieffer, *New J. Phys.* **13**, 033017 (2011).
- ²²V. Malka, S. Fritzler, E. Lefebvre, M.-M. Aeonard, F. Burgy, J.-P. Chambaret, J.-F. Chemin, K. Krushelnick, G. Malka, S. P. D. Mangles, Z. Najmudin, M. Pittman, J.-P. Rousseau, J.-N. Scheurer, B. Walton, and A. E. Dangor, *Science* **298**, 1596 (2002).
- ²³S. Kneip, C. McGuffey, F. Dollar, M. S. Bloom, V. Chvykov, G. Kalintchenko, K. Krushelnick, A. Maksimchuk, S. P. D. Mangles, T. Matsuoka, Z. Najmudin, C. A. J. Palmer, J. Schreiber, W. Schumaker, A. G. R. Thomas, and V. Yanovsky, *Appl. Phys. Lett.* **99**, 093701 (2011).
- ²⁴C. McGuffey, T. Matsuoka, S. Kneip, W. Schumaker, F. Dollar, C. Zulick, V. Chvykov, G. Kalintchenko, V. Yanovsky, A. Maksimchuk, A. G. R. Thomas, K. Krushelnick, and Z. Najmudin, *Phys. Plasmas* **19**, 063113 (2012).
- ²⁵W. Lu, M. Tzoufras, C. Joshi, F. S. Tsung, W. B. Mori, J. Vieira, R. A. Fonseca, and L. O. Silva, *Phys. Rev. ST Accel. Beams* **10**, 061301 (2007).
- ²⁶A. G. R. Thomas, M. Sherlock, C. Kuranz, C. P. Ridgers, and R. P. Drake, *New J. Phys.* **15**, 015017 (2013).
- ²⁷A. Pak, K. A. Marsh, S. F. Martins, W. Lu, W. B. Mori, and C. Joshi, *Phys. Rev. Lett.* **104**, 025003 (2010); C. McGuffey, A. G. R. Thomas, W. Schumaker, T. Matsuoka, V. Chvykov, F. J. Dollar, G. Kalintchenko, V. Yanovsky, A. Maksimchuk, K. Krushelnick, V. Y. Bychenkov, I. V. Glazyrin, and A. V. Karpeev, *ibid.* **104**, 025004 (2010).